

High-order kinetic flux vector splitting schemes in general coordinates for ideal quantum gas dynamics

Jaw-Yen Yang ^{a,*}, Tse-Yang Hsieh ^a, Yu-Hsin Shi ^a, Kun Xu ^b

^a *Institute of Applied Mechanics, National Taiwan University, Taipei, Taiwan*

^b *The Hong Kong University of Science and Technology, Clear Water Bay, Kowloon, Hong Kong*

Received 16 December 2006; received in revised form 11 July 2007; accepted 22 August 2007

Available online 31 August 2007

Abstract

A class of high-order kinetic flux vector splitting schemes are presented for solving ideal quantum gas dynamics based on quantum statistical mechanics. The collisionless quantum Boltzmann equation approach is adopted and both Bose–Einstein and Fermi–Dirac gases are considered. The formulas for the split flux vectors are derived based on the general three-dimensional distribution function in velocity space and formulas for lower dimensions can be directly deduced. General curvilinear coordinates are introduced to treat practical problems with general geometry. High-order accurate schemes using weighted essentially non-oscillatory methods are implemented. The resulting high resolution kinetic flux splitting schemes are tested for 1D shock tube flows and shock wave diffraction by a 2D wedge and by a circular cylinder in ideal quantum gases. Excellent results have been obtained for all examples computed.

© 2007 Elsevier Inc. All rights reserved.

Keywords: Ideal quantum gas; Quantum gas dynamics; KFVS scheme; High resolution scheme; General coordinates

1. Introduction

Recently, a class of kinetic flux vector splitting (KFVS) schemes have been derived for the ideal quantum gas dynamics [26] based on the quantum collisionless Boltzmann equation and BGK model [1]. Formulations in Cartesian coordinates have been derived starting from one- to three-dimensional (in velocity or momentum space) distribution functions. The derivations of the split flux vectors for the lower dimensions, i.e., less than three space dimensions, are done based on one- and two-dimensional reduced equilibrium distribution functions. Both Bose–Einstein and Fermi–Dirac gases have been considered. It is well known that the effects of dimensionality are important attributes that are characteristic of the ideal quantum gases, see [16]. In this paper, we further extend and generalize the method to general coordinates and adopt a more general three-dimensional (in velocity space) distribution approach to derive the split flux vectors for the ideal quantum gas dynamics. The formulas for lower dimensions can be directly deduced. The resulting split flux vectors

* Corresponding author. Tel.: +886 2 3366 5636; fax: +886 2 2362 9290.

E-mail address: yangjy@iam.ntu.edu.tw (J.-Y. Yang).

based on the present approach share the same form as the previous ones but with different orders of boson or fermion functions.

In statistical mechanics, there are three kinds of equilibrium distributions for a system of N identical particles, namely, the Maxwell–Boltzmann (MB), Bose–Einstein (BE) and Fermi–Dirac (FD) distributions; the former one is for classical particles and the later two are for quantum particles. The physical properties of fermion and boson systems are profoundly different at sufficiently low temperature. However, in the classical limit, both quantum distributions reduce to the Maxwell–Boltzmann distribution. The ideal classical gas dynamics can be described by the Maxwell–Boltzmann distribution which corresponding to the lowest order solution of the classical Boltzmann equation when Chapman–Enskog procedure is employed [2]. The conservation laws based on the Maxwell–Boltzmann distribution is the well-known Euler equations of classical gas dynamics. Analogous to the classical Boltzmann equation, a quantum Boltzmann equation for the transport phenomenon can be developed for fermions and bosons, see [11]. A formal solution procedure which generalizing the Chapman–Enskog method to solve the quantum Boltzmann equation was given by Uehling and Uhlenbeck [20] where the first and second approximations of the distribution function and expressions for the viscosity and heat conductivity coefficients were given. Thus, the corresponding quantum gas dynamics as governed by the quantum Euler equations and quantum Navier–Stokes equations can also be explored based on the quantum kinetic theory.

In the past 40 years, extensive theoretical and computational methods have been developed to solve the Euler equations of classical gas dynamics see [8,19]. A particular class of methods closely related to the present work are the KFVS of [4,5,17]. More recent works on kinetic numerical methods have been given by Xu and co-workers [14,21–23]. An interesting explicit scheme for solving the ideal gas dynamics, the so-called beam scheme has been presented by Sanders and Predergast [18] for solving the equilibrium limit of the classical Boltzmann equation. In contrast to the beam scheme which was based on the local thermodynamic equilibrium solution of the Boltzmann equation, the derivation of KFVS method is based on the collisionless Boltzmann equation and results a novel method for solving the transport processes governed by the Euler equations of Newtonian gas dynamics. Both the basic beam scheme and the KFVS scheme for the classical Euler equations are of first order accuracy and thus numerically diffusive, although with different degrees of numerical diffusion. However, this numerical diffusion of first order beam and KFVS (or any upwind) methods can be significantly reduced by the implementation of higher-order methods. A corresponding beam scheme for ideal quantum gas dynamics has been given [25]. In this work, we shall adopt and generalize the concept of KFVS scheme to devise a numerical method for the computation of ideal quantum gas dynamics. We start with the quantum Boltzmann equation, in which the particles obey the quantum statistics. First, the KFVS scheme for ideal quantum gas dynamics is derived based on solution of the initial value problem of the collisionless quantum Boltzmann equation. The main difference between the present work and our previous one [26] lies in the use of three-dimensional distribution function in velocity space through out here even for derivation of formulas for lower dimensions. This difference results in that the split flux vectors are expressed in terms of different orders of the Bose functions or Fermi functions. The present approach allows very systematic derivations for the split fluxes in various space dimensions. To increase the accuracy, we adopt the weighted essentially non-oscillatory (WENO) method [10] into our basic first order KFVS scheme to yield a class of high-order KFVS schemes for computing ideal quantum gas dynamical flows. Although there are some recent works [7,24] in which improvement and refinement of the original WENO method have been made, however, we are not experimenting it here, since our purpose in this work is not to develop or compare different WENO methods. In view of the existing extensive works on experimental and computational classical gas dynamics, the present quantum KFVS schemes can be potentially useful for revealing various dynamical aspects of ideal quantum gas through mathematical and physical analogies. In addition, this work also provides a framework for parallel treatment of molecules, electrons, phonons, and photons in equilibrium carrier transport [3].

The paper is organized as following. We first describe the elements of quantum Boltzmann transport equation in Section 2. The basic kinetic flux splitting method is derived in Section 3 for the bosons and fermions. General curvilinear coordinates are introduced to treat general geometries. Treatment of boundary conditions is also outlined. In Section 4, the weighted ENO method is implemented to yield a class of high-order flux

vector splitting methods. In Section 5, numerical experiments in one and two space dimensions are given to illustrate the methods. Lastly, some concluding remarks are given in Section 6.

2. Collisionless quantum Boltzmann equation

In this section, elements of the semi-classical Boltzmann transport equation appropriate for the development of present work are briefly outlined. Following Kadanoff and Baym [11], we consider the quantum Boltzmann equation

$$\left(\frac{\partial}{\partial t} + \vec{u} \cdot \nabla_{\vec{x}} - \nabla V(\vec{x}, t) \cdot \nabla_{\vec{u}}\right) f(\vec{x}, \vec{u}, t) = \left(\frac{\delta f}{\delta t}\right)_{\text{collision}}, \tag{1}$$

where \vec{u} is the particle velocity, V is the externally applied field and $f(\vec{x}, \vec{u}, t)$ is the distribution function which represents the average density of particles with velocity \vec{u} at the space–time point \vec{x}, t . The $(\delta f/\delta t)_{\text{collision}}$ denotes the collision term. A formal solution procedure which generalizing the Chapman–Enskog method to solve Eq. (1) was given by Uehling and Uhlenbeck [20]. In recent years, the development of numerical methods for solving the quantum Boltzmann equation has become an active research subject, see [6]. A recent review on the numerical methods for the dynamics and transport of atomic quantum gases has been given (see [13] and the references therein). The major mathematical difficulty of solving Eq. (1) is due to the nonlinear collision term. Here, we consider only the cases where the collision term can be neglected and demand that

$$\left(\frac{\delta f}{\delta t}\right)_{\text{collision}} = 0. \tag{2}$$

This corresponds to two important special cases. One is the free molecular flow (where the mean free path of the gas system is very large or infinite) and the other is the equilibrium flow (where the mean collision time is infinitely short). The solution to Eq. (1) for the equilibrium flow is given by

$$f(\vec{x}, \vec{u}, t) = f_0 = \frac{m^4}{h^3} \frac{1}{\exp\left(\lambda(\vec{u} - \vec{U})^2 - \mu/k_B T\right) + \theta} = \frac{m^4}{h^3} \frac{1}{z^{-1} \exp\left(\lambda(\vec{u} - \vec{U})^2\right) + \theta}, \tag{3}$$

where $\lambda = m/2k_B T$ and $\theta = +1$ denotes the Fermi–Dirac statistics and $\theta = -1$ the Bose–Einstein statistics. The equilibrium distribution is an important reference state since most transport phenomena in gases originate from its slightly deviation from the equilibrium state. To complete the equilibrium solution we have to determine the unknown functions, namely, the gas temperature, $T(\vec{x}, t)$, the mean velocity, $\vec{U}(\vec{x}, t) = (U, V, W)$, and the chemical potential, μ , or fugacity, $z = \exp(\mu/k_B T)$, which appear in Eq. (3). These flow parameters can be determined by making use of the conservation laws for number of particles, momentum, and energy. These conservation laws can be obtained by multiplying Eq. (1) by 1, \vec{u} , and $\vec{u}^2/2$, and then integrating the resulting equations over the particle velocity space $\vec{u} = (u, v, w)$. The integrals of the collision terms in all three cases vanish automatically and we have the differential conservation laws for the conserved macroscopic quantities, i.e., the density ρ , momentum $\rho\vec{U}$, and energy density $\rho\epsilon$ as follows:

$$\frac{\partial \rho}{\partial t} + \nabla_{\vec{x}} \cdot \rho\vec{U} = 0, \tag{4}$$

$$\frac{\partial \rho\vec{U}}{\partial t} + \nabla_{\vec{x}} \cdot \int \vec{u}\vec{u}f(\vec{x}, \vec{u}, t) d\vec{u} = -\rho\nabla_{\vec{x}}V, \tag{5}$$

$$\frac{\partial \rho\epsilon}{\partial t} + \nabla_{\vec{x}} \cdot \int \vec{u} \frac{\vec{u}^2}{2} f(\vec{x}, \vec{u}, t) d\vec{u} = -\rho\vec{U} \cdot \nabla_{\vec{x}}V, \tag{6}$$

where $(\rho, \rho\vec{U}, \rho\epsilon)$ are the moments of $\phi_{\alpha} = (1, \vec{u}, \vec{u}^2/2)$ and for the equilibrium case, they can be explicitly calculated as

$$\rho(\vec{x}, t) = \int f_0(\vec{x}, \vec{u}, t) d\vec{u} = \frac{m}{\Lambda^3} Q_{\frac{3}{2}}(z), \tag{7}$$

$$\rho(\vec{x}, t)\vec{U}(\vec{x}, t) = \int \vec{u}f_0(\vec{x}, \vec{u}, t) d\vec{u} = \frac{m}{\Lambda^3} Q_{\frac{3}{2}}(z)\vec{U}, \tag{8}$$

$$\rho(\vec{x}, t)\epsilon(\vec{x}, t) = \int \frac{\vec{u}^2}{2}f_0(\vec{x}, \vec{u}, t) d\vec{u} = \frac{3}{2} \frac{m}{\beta\Lambda^3} Q_{\frac{5}{2}}(z) + \frac{1}{2} \frac{m}{\Lambda^3} Q_{\frac{3}{2}}(z)\vec{U}^2 = \frac{1}{\gamma - 1}P(\vec{x}, t) + \frac{1}{2}\rho(\vec{x}, t)\vec{U}^2, \tag{9}$$

where $\Lambda = h\sqrt{\lambda/\pi}/m$ is the thermal wavelength, $P(\vec{x}, t)$ is the gas pressure and γ is the ratio of specific heats. In the above, $Q_\nu(z)$ denotes the quantum integration function of order ν which is defined by

$$Q_\nu(z) = \begin{cases} \mathcal{G}_\nu(z), & \text{for Bose gas,} \\ \mathcal{F}_\nu(z), & \text{for Fermi gas,} \end{cases} \tag{10}$$

where $\mathcal{G}_\nu(z)$ denotes the Bose–Einstein integral and $\mathcal{F}_\nu(z)$ denotes the Fermi–Dirac integral of order ν , respectively:

$$\mathcal{G}_\nu(z) \equiv \frac{1}{\Gamma(\nu)} \int_0^\infty \frac{x^{\nu-1}}{z^{-1}e^x - 1} dx = \sum_{l=1}^\infty \frac{z^l}{l^\nu}, \tag{11}$$

$$\mathcal{F}_\nu(z) \equiv \frac{1}{\Gamma(\nu)} \int_0^\infty \frac{x^{\nu-1}}{z^{-1}e^x + 1} dx = \sum_{l=1}^\infty \frac{-(-z)^l}{l^\nu}, \tag{12}$$

and $\Gamma(\nu)$ is gamma function.

Other higher-order moments such as stress tensor and the heat flux vector can also be defined. For the local equilibrium solution, one can obtain these macroscopic quantities in closed form in terms of Bose or Fermi functions [9,15]. In the following derivation of the KFVS method, the equilibrium state will serve only as the initial state for the free gas evolution according to the collisionless Boltzmann equation. We also neglect the external potential $V(\vec{x})$ here which can be included as that done in [26].

3. The quantum KFVS scheme

In this section, the basic KFVS scheme is derived based on the collisionless Boltzmann equation for a quantum gas. To illustrate the method, we first consider the flow problems in one space dimension where $(\vec{U} = (U, 0, 0))$. Divide the space into a number of uniform cells. Each cell occupies a small space $x \in [x_{i-\frac{1}{2}}, x_{i+\frac{1}{2}}]$, where $x_{i+1/2}$ denotes the cell interface between cells i and $i + 1$, and the cell center is located at x_i . With the initial mass, momentum and energy densities given inside each cell i :

$$\mathbf{W}_i = (\rho_i, \rho_i U_i, \rho_i \epsilon_i), \tag{13}$$

and the fugacity z can be obtained from Eqs. (7) and (9) through the following relation:

$$2(\rho\epsilon) - \left(\frac{h^2}{2\pi m^{5/3}}\right) \left(\frac{\rho}{Q_{\frac{3}{2}}(z)}\right)^{5/3} Q_{\frac{5}{2}}(z) - \frac{(\rho U)^2}{\rho} = 0. \tag{14}$$

Once we have obtained the fugacity, the temperature (or λ) can be calculated. We can then define an equilibrium state f_0 for the quantum gas, which is

$$f_0 = \frac{m^4}{h^3} \frac{1}{z^{-1} \exp[\lambda((u - U)^2 + v^2 + w^2)] + \theta}. \tag{15}$$

It is noted that the distribution function is in three-dimensional velocity space (u, v, w) and the integration over the velocity space to obtain the macroscopic flow variables is done in three-dimensional manner.

The initial value problem of the collisionless Boltzmann equation in one space dimension is described by

$$\frac{\partial f}{\partial t} + u \frac{\partial f}{\partial x} = 0 \tag{16}$$

with the initial condition around the cell interface at $x = x_{i+1/2}$

$$f(x, u, v, w, t = 0) = \begin{cases} f_{0,i}, & x \leq x_{i+\frac{1}{2}}, \\ f_{0,i+1}, & x > x_{i+\frac{1}{2}}. \end{cases} \tag{17}$$

The solution of the above initial value problem, $f(x, u, v, w, t)$ at $x_{i+1/2}$ and time t , becomes

$$f\left(x_{i+\frac{1}{2}}, u, v, w, t\right) = \begin{cases} f_{0,i}, & u \geq 0, \\ f_{0,i+1}, & u < 0. \end{cases} \tag{18}$$

From the above distribution function, the numerical fluxes for the mass, momentum and energy across the cell interface can be constructed, which are

$$\begin{aligned} F_{i+\frac{1}{2}} &= \begin{pmatrix} F_\rho \\ F_{\rho U} \\ F_{\rho e} \end{pmatrix}_{i+\frac{1}{2}} = \int \int \int u \psi_\alpha f(x_{i+\frac{1}{2}}, u, v, w, t) du dv dw \\ &= \int \int \int_{u \geq 0} u \psi_\alpha f_{0,i} du dv dw + \int \int \int_{u < 0} u \psi_\alpha f_{0,i+1} du dv dw = F_i^+ + F_{i+1}^-, \end{aligned} \tag{19}$$

where ψ_α stands for the moments $\psi_\alpha = (1, u, u^2/2)$.

It is noted that even for the one-dimensional problems, the integration here is done with respect to u, v , and w spaces instead of just one-dimensional integration as given previously [26] where the reduced distribution function in lower dimension was used.

The detailed expressions of the split fluxes can be directly obtained and they are

$$F^\pm = \begin{pmatrix} F_\rho^\pm \\ F_{\rho U}^\pm \\ F_{\rho e}^\pm \end{pmatrix} = \begin{pmatrix} \rho U a^\pm(U) \pm \rho b(U) \\ P c^\pm(U) + U(\rho U a^\pm(U) \pm \rho b(U)) \\ \frac{5}{2} P U c^\pm(U) \pm 2 P d(U) + \frac{1}{2} U^2(\rho U a^\pm(U) \pm \rho b(U)) \end{pmatrix}, \tag{20}$$

where the functions $a^\pm(U)$, $b(U)$, $c^\pm(U)$ and $d(U)$ are defined by

$$a^\pm(U) = \frac{1}{2} \left(1 \pm \frac{\tilde{Q}_2(s(U), z)}{Q_2(z)} \right), \tag{21}$$

$$b(U) = \frac{1}{2\sqrt{\pi\lambda}} \frac{\tilde{Q}_2(s(U), z)}{Q_2(z)}, \tag{22}$$

$$c^\pm(U) = \frac{1}{2} \left(1 \pm \frac{\tilde{Q}_3(s(U), z)}{Q_3(z)} \right), \tag{23}$$

$$d(U) = \frac{1}{2\sqrt{\pi\lambda}} \frac{\tilde{Q}_3(s(U), z)}{Q_3(z)}, \tag{24}$$

where $s(U) = \sqrt{\lambda}U$ and $\tilde{Q}_v(s, z)(\tilde{\tilde{Q}}_v(s, z)) = \tilde{G}_v(s, z)(\tilde{\tilde{G}}_v(s, z))$ for a Bose gas and $\tilde{Q}_v(s, z)(\tilde{\tilde{Q}}_v(s, z)) = \tilde{F}_v(s, z)(\tilde{\tilde{F}}_v(s, z))$ for a Fermi gas, where

$$\tilde{G}_v(s, z) = \sum_{l=1}^{\infty} \operatorname{erf}(\sqrt{l}s) \frac{z^l}{l^v}, \tag{25}$$

$$\tilde{F}_v(s, z) = \sum_{l=1}^{\infty} \operatorname{erf}(\sqrt{l}s) \frac{-(-z)^l}{l^v}, \tag{26}$$

$$\tilde{\tilde{G}}_v(s, z) = \sum_{l=1}^{\infty} \exp(-ls^2) \frac{z^l}{l^v}, \tag{27}$$

$$\widetilde{\mathcal{F}}_v(s, z) = \sum_{l=1}^{\infty} \exp(-ls^2) \frac{-(-z)^l}{l^v}. \tag{28}$$

Using the above numerical fluxes, the flow variables ρ_i , $\rho_i U_i$, and $\rho_i \epsilon_i$ inside each cell can be updated as:

$$\mathbf{W}_i^{n+1} = \mathbf{W}_i^n - \frac{\Delta t}{\Delta x} \left(F_{i+\frac{1}{2}}^{(1)} - F_{i-\frac{1}{2}}^{(1)} \right); \quad F_{i+\frac{1}{2}}^{(1)} = F_i^+ + F_{i+1}^-, \tag{29}$$

where n is the time step number, Δt is the time step size, and Δx is the mesh size.

The time step size can be chosen by Courant–Friedrichs–Lewy (CFL) stability condition:

$$\sigma \leq \frac{1}{\max(|U| + 3C)}, \tag{30}$$

where C is the local speed of sound

$$C = \sqrt{\gamma \frac{P}{\rho}}. \tag{31}$$

The corresponding formulas for two and three space dimensions in Cartesian coordinates can be similarly derived as above with the mean velocity vector $\vec{U}(x, y, t) = (U, V, 0)$ and $\vec{U}(x, y, z, t) = (U, V, W)$, respectively.

To treat general geometries, one usually casts the equations in curvilinear coordinates. Here, we derive the formulas for the split fluxes in two space dimensions in (ξ, η) curvilinear coordinates. Divide the computational domain into uniform rectangular cells (with $\Delta \xi = \Delta \eta = 1$) and denote each cell as (i, j) . Define the unit normal and the contravariant velocities as:

$$\left(\hat{\xi}_x, \hat{\xi}_y \right) = \frac{(\xi_x, \xi_y)}{\sqrt{\xi_x^2 + \xi_y^2}}, \quad \left(\hat{\eta}_x, \hat{\eta}_y \right) = \frac{(\eta_x, \eta_y)}{\sqrt{\eta_x^2 + \eta_y^2}}, \tag{32}$$

$$\hat{U} = \hat{\xi}_x U + \hat{\xi}_y V, \quad \hat{V} = \hat{\eta}_x U + \hat{\eta}_y V. \tag{33}$$

Then the split fluxes in the generalized coordinates (ξ, η) are given, respectively, by

$$\hat{F}^{\pm} = \begin{pmatrix} \hat{F}_{\rho}^{\pm} \\ \hat{F}_{\rho U}^{\pm} \\ \hat{F}_{\rho V}^{\pm} \\ \hat{F}_{\rho \epsilon}^{\pm} \end{pmatrix} = \begin{pmatrix} \rho \hat{U} a^{\pm}(\hat{U}) \pm \rho b(\hat{U}) \\ \hat{\xi}_x P c^{\pm}(\hat{U}) + U(\rho \hat{U} a^{\pm}(\hat{U}) \pm \rho b(\hat{U})) \\ \hat{\xi}_y P c^{\pm}(\hat{U}) + V(\rho \hat{U} a^{\pm}(\hat{U}) \pm \rho b(\hat{U})) \\ \frac{\xi}{2} P \hat{U} c^{\pm}(\hat{U}) + 2Pd(\hat{U}) + \frac{1}{2}(U^2 + V^2)(\rho \hat{U} a^{\pm}(\hat{U}) \pm \rho b(\hat{U})) \end{pmatrix}, \tag{34}$$

$$\hat{G}^{\pm} = \begin{pmatrix} \hat{G}_{\rho}^{\pm} \\ \hat{G}_{\rho U}^{\pm} \\ \hat{G}_{\rho V}^{\pm} \\ \hat{G}_{\rho \epsilon}^{\pm} \end{pmatrix} = \begin{pmatrix} \rho \hat{V} a^{\pm}(\hat{V}) \pm \rho b(\hat{V}) \\ \hat{\eta}_x P c^{\pm}(\hat{V}) + U(\rho \hat{V} a^{\pm}(\hat{V}) \pm \rho b(\hat{V})) \\ \hat{\eta}_y P c^{\pm}(\hat{V}) + V(\rho \hat{V} a^{\pm}(\hat{V}) \pm \rho b(\hat{V})) \\ \frac{\eta}{2} P \hat{V} c^{\pm}(\hat{V}) + 2Pd(\hat{V}) + \frac{1}{2}(U^2 + V^2)(\rho \hat{V} a^{\pm}(\hat{V}) \pm \rho b(\hat{V})) \end{pmatrix}, \tag{35}$$

where expressions of a^{\pm} , b , c^{\pm} , and d are given in Eqs. (21)–(24).

Using the above split fluxes, the conservative flow variables, $\mathbf{W} = (\rho, \rho U, \rho V, \rho \epsilon)_{i,j}$ inside each cell (i, j) can be updated as:

$$\mathbf{W}_{i,j}^{n+1} = \mathbf{W}_{i,j}^n - \frac{\Delta t}{\Delta \xi} \left(\hat{F}_{i+\frac{1}{2},j}^{(1)} - \hat{F}_{i-\frac{1}{2},j}^{(1)} \right) - \frac{\Delta t}{\Delta \eta} \left(\hat{G}_{i,j+\frac{1}{2}}^{(1)} - \hat{G}_{i,j-\frac{1}{2}}^{(1)} \right), \tag{36}$$

where

$$\hat{F}_{i+\frac{1}{2},j}^{(1)} = \hat{F}_{i,j}^+ + \hat{F}_{i+1,j}^-, \quad \hat{G}_{i,j+\frac{1}{2}}^{(1)} = \hat{G}_{i,j}^+ + \hat{G}_{i,j+1}^-. \tag{37}$$

The corresponding split fluxes for three space dimensions in curvilinear coordinates (ξ, η, ζ) can be similarly derived and they are given in Appendix A.

At this stage, we have completed the description of the first-order KFVS scheme for the quantum gas.

Before ending this section, a brief descriptions regarding to the boundary conditions used are given below. For the problems considered in this work, two types of boundary conditions, far field and solid wall, are encountered. For inviscid flow, the zero normal velocity boundary condition is warranted on a solid wall. To be specific, we use the problem of shock wave reflection by a cylinder as example in which the cylinder wall is at $j = 1$ and the outer far field boundary at $j = J$. Due to the finite computational domain used, a non-reflecting boundary condition at the far field boundary needs to be employed. The upwinding feature of the basic flux vector splitting scheme provides a natural way to achieve this. At the far field boundary, we have

$$\mathbf{W}_{i,J}^* = \mathbf{W}_{i,J}^n - \Delta t \left(\widehat{G}_{i,J}^+ - \widehat{G}_{i,J-1}^+ \right). \tag{38}$$

At the cylinder surface, we have

$$\mathbf{W}_{i,1}^* = \mathbf{W}_{i,1}^n - \Delta t \left(\widehat{G}_{i,2}^- - \widehat{G}_{i,1}^- \right). \tag{39}$$

The above boundary integration only partially updates the state vector since the information carried by the positive (for $j = 1$) eigenvalues is not counted and additional conditions are needed to supplement in order to completely update the state vector at the new time level. The boundary conditions on the cylinder ($j = 1$) are as follow:

$$\widehat{V}_\eta^{n+1} - \frac{2c^{n+1}}{g} = \widehat{V}_\eta^* - \frac{2c^*}{g}, \tag{40}$$

$$\frac{P^{n+1}}{(\rho^{n+1})^{g+1}} = \frac{P^*}{(\rho^*)^{g+1}}, \tag{41}$$

$$\widehat{U}_\eta^{n+1} = \widehat{U}_\eta^*, \tag{42}$$

and the surface tangency condition

$$\widehat{V}_\eta^{n+1} = 0, \tag{43}$$

where $\widehat{V}_\eta = \widehat{V}/|\nabla\eta|$ and $\widehat{U}_\eta = (\eta_x U - \eta_x V)/|\nabla\eta|$.

For two-dimensional problem, we have $g = 1$ when the equation of state is used [15].

A simple way to satisfy the zero normal velocity condition on the wall is to use the reflection principle, i.e., $\rho, \rho\widehat{V}$ and ϵ are taken to be symmetric and $\rho\widehat{U}$ is antisymmetric across the cell interface, with \widehat{U} and \widehat{V} being the local normal and tangential components of the velocity vector. In this way, the values of the state vector in any number of dummy cells can be specified.

4. Implementation of WENO schemes

We shall give the detailed expressions for the numerical flux in one dimension only (say, ξ -direction) and the expressions for the η -direction can be similarly defined. For the purpose of implementing high-order methods we can further express the basic quantum KFVS scheme (without external potential) defined by Eq. (29) in terms of numerical flux as follows:

$$\mathbf{W}_i^{n+1} = \mathbf{W}_i^n - \sigma \left(F_{i+1/2}^N - F_{i-1/2}^N \right), \tag{44}$$

where the numerical flux $F_{i+1/2}^N$ for the basic first order KFVS scheme is given in Eq. (29).

The above scheme is of first-order accuracy and thus is very diffusive. In practical applications we need high-order methods. In this section, we adopt the weighted essentially non-oscillatory interpolation method [12,10] to the basic first order quantum KFVS scheme to result in a class of high resolution methods for computing of quantum ideal gas dynamical flows. In recent years, some works such as mapped WENO [7] and

anti-diffusion WENO [24] have been developed, which improve and refine the original WENO method. Although we can also implement these new WENO variants, however, we are not experimenting it here. The numerical flux is further expressed as:

$$F_{i+1/2}^N = F_{i+1/2}^{N+} + F_{i+1/2}^{N-}. \quad (45)$$

Here, we consider a fifth-order accurate ($r = 3$) WENO scheme for the spatial difference of numerical fluxes. The WENO scheme for $r = 3$, denoted as WENO3, can be expressed as:

$$F_{i+1/2}^{N+} = \omega_0^+ \left(\frac{2}{6} F_{i-2}^+ - \frac{7}{6} F_{i-1}^+ + \frac{11}{6} F_i^+ \right) + \omega_1^+ \left(-\frac{1}{6} F_{i-1}^+ + \frac{5}{6} F_i^+ + \frac{2}{6} F_{i+1}^+ \right) + \omega_2^+ \left(\frac{2}{6} F_i^+ + \frac{5}{6} F_{i+1}^+ - \frac{1}{6} F_{i+2}^+ \right), \quad (46)$$

$$\omega_k^+ = \frac{\alpha_k^+}{\alpha_0^+ + \alpha_1^+ + \alpha_2^+}, \quad k = 0, 1, 2, \quad (47)$$

$$\alpha_0^+ = \frac{1}{10(\epsilon + IS_0^+)^2}, \quad \alpha_1^+ = \frac{6}{10(\epsilon + IS_1^+)^2}, \quad \alpha_2^+ = \frac{3}{10(\epsilon + IS_2^+)^2}, \quad (48)$$

$$\begin{aligned} IS_0^+ &= \frac{13}{12} (F_{i-2}^+ - 2F_{i-1}^+ + F_i^+)^2 + \frac{1}{4} (F_{i-2}^+ - 4F_{i-1}^+ + 3F_i^+)^2, \\ IS_1^+ &= \frac{13}{12} (F_{i-1}^+ - 2F_i^+ + F_{i+1}^+)^2 + \frac{1}{4} (F_{i-1}^+ - F_{i+1}^+)^2, \\ IS_2^+ &= \frac{13}{12} (F_i^+ - 2F_{i+1}^+ + F_{i+2}^+)^2 + \frac{1}{4} (3F_i^+ - 4F_{i+1}^+ + F_{i+2}^+)^2. \end{aligned} \quad (49)$$

The numerical flux for the negative part is given by

$$F_{j+1/2}^{N-} = \omega_0^- \left(-\frac{1}{6} F_{i-1}^- + \frac{5}{6} F_i^- + \frac{2}{6} F_{i+1}^- \right) + \omega_1^- \left(\frac{2}{6} F_i^- + \frac{5}{6} F_{i+1}^- - \frac{1}{6} F_{i+2}^- \right) + \omega_2^- \left(\frac{11}{6} F_{i+1}^- - \frac{7}{6} F_{i+2}^- + \frac{2}{6} F_{i+3}^- \right), \quad (50)$$

$$\omega_k^- = \frac{\alpha_k^-}{\alpha_0^- + \alpha_1^- + \alpha_2^-}, \quad k = 0, 1, 2, \quad (51)$$

$$\alpha_0^- = \frac{3}{10(\epsilon + IS_0^-)^2}, \quad \alpha_1^- = \frac{6}{10(\epsilon + IS_1^-)^2}, \quad \alpha_2^- = \frac{1}{10(\epsilon + IS_2^-)^2}, \quad (52)$$

$$\begin{aligned} IS_0^- &= \frac{13}{12} (F_{i-1}^- - 2F_i^- + F_{i+1}^-)^2 + \frac{1}{4} (F_{i-1}^- - 4F_i^- + 3F_{i+1}^-)^2, \\ IS_1^- &= \frac{13}{12} (F_i^- - 2F_{i+1}^- + F_{i+2}^-)^2 + \frac{1}{4} (F_i^- - F_{i+2}^-)^2, \\ IS_2^- &= \frac{13}{12} (F_{i+1}^- - 2F_{i+2}^- + F_{i+3}^-)^2 + \frac{1}{4} (3F_{i+1}^- - 4F_{i+2}^- + F_{i+3}^-)^2. \end{aligned} \quad (53)$$

It is noted that the present implementation of WENO methods for the KFVS scheme is directly operating on the split fluxes F^\pm and there is no need to project the state variables to the characteristic space as required by other approximate Riemann solvers.

In the following, we shall denote KFVS–WENO3 as the KFVS scheme with WENO3 implementation.

5. Numerical experiments

In this section, we report several numerical examples to illustrate the present quantum KFVS methods and the effects of high-order WENO schemes. Both one- and two-dimensional flows are considered. For two-dimensional flows, the general coordinates are employed. In the 1D shock tube problem, a diaphragm, which is located at $x = 0.5$, separating two regions, each remains at a constant equilibrium state, initially at $t = 0$. The macroscopic properties on both sides of the diaphragm are set at different values to present different cases.

For the 2D shock wave diffraction problem, the initial position of the incident shock wave is arbitrarily located at certain distance to the left of the wedge or the circular cylinder. The conditions ahead of (state 1) and behind (state 2) a moving shock are related by

$$\frac{P_2}{P_1} = \frac{2\gamma M_s^2 - (\gamma - 1)}{\gamma + 1}, \tag{54}$$

$$\frac{\rho_2}{\rho_1} = \frac{G(P_2/P_1) + 1}{G + (P_2/P_1)}, \tag{55}$$

$$U_2 = M_s \left[1 - \frac{(\gamma - 1)M_s^2 + 2}{(\gamma + 1)M_s^2} \right] c_1, \tag{56}$$

where $G = (\gamma + 1)/(\gamma - 1)$ and $c_1 = (\gamma P_1/\rho_1)^{1/2}$.

Initially, when $t = 0$, the fugacity at state 1 (z_1) is assigned, then ρ_1, P_1, T_1 and ϵ_1 can be calculated by the following equations which are derived from the state equation with an assigned value of M_s and a given value of γ for a particular quantum gas:

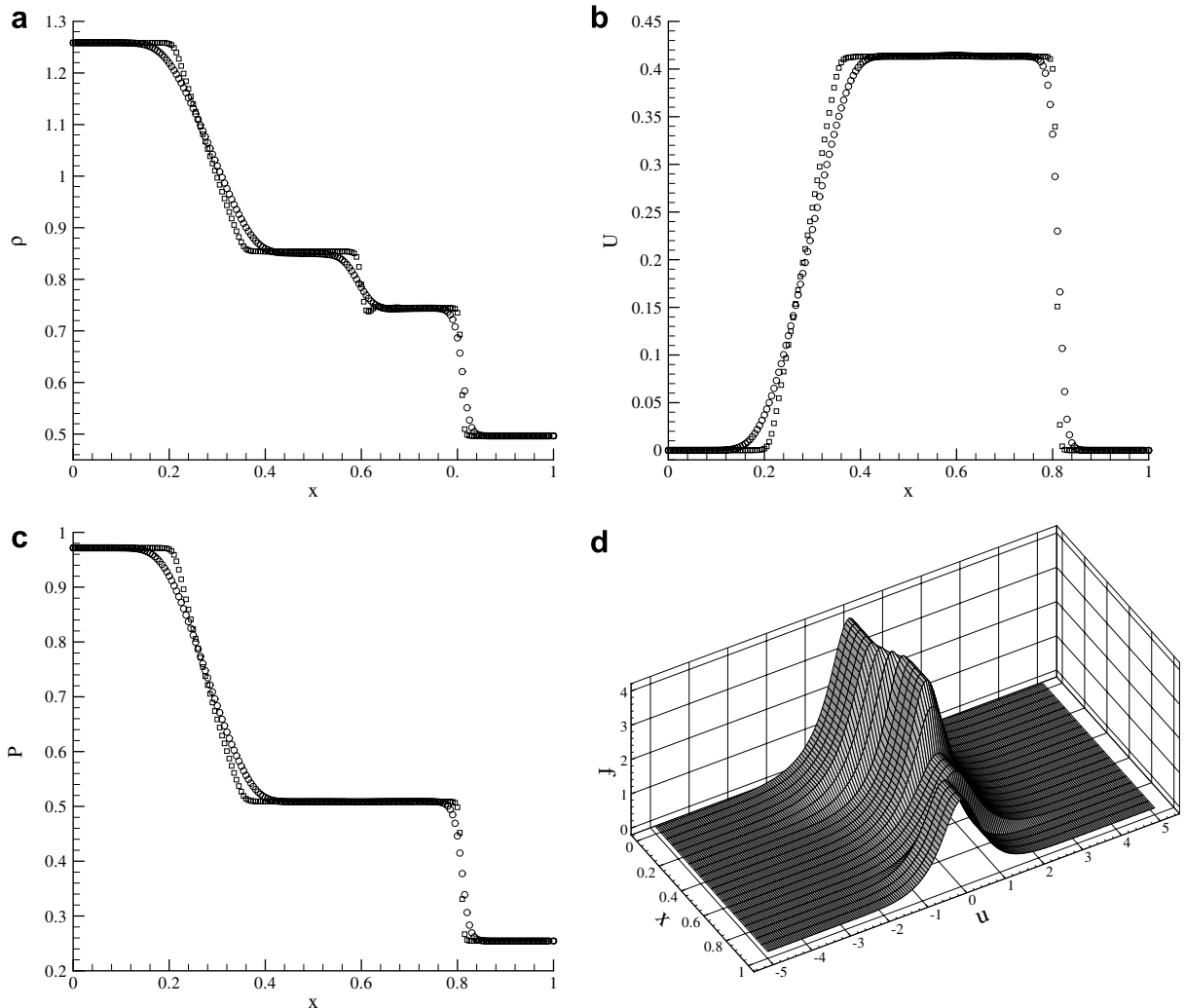


Fig. 1. Quantum shock tube solution, Bose gas: 1st order (○) and WENO3 (□).

$$T_1 = \frac{Q_{3/2}(z_1)}{Q_{5/2}(z_1)\gamma}, \quad \rho_1 = T_1^{3/2} Q_{3/2}(z_1), \quad P_1 = \frac{\rho_1}{\gamma}, \tag{57}$$

$$\epsilon_1 = \frac{P_1}{\gamma\rho_1} + \frac{1}{2}\rho_1(U_1^2 + V_1^2). \tag{58}$$

The velocity components of state 1 are set to zero, $U_1 = V_1 = 0$. The conditions at state 2 are calculated by Eqs. (54)–(58) and the energy density ϵ_2 , temperature T_2 and fugacity z are given as previous procedure.

Moving shock relations are applied to both sides of the incident shock and the consequent movement of motion is simulated without imposing any explicit equation of motion for the incident shock.

Example 1 (1D shock tube problem: boson gas). The initial condition is specified as $\mathbf{W}_L = (\rho_L, \rho_L U_L, \rho_L \epsilon_L) = (1.259, 0.0, 1.458)$ for $0 < x \leq 0.5$ and $\mathbf{W}_R = (\rho_R, \rho_R U_R, \rho_R \epsilon_R) = (0.496, 0.0, 0.382)$ for $0.5 < x < 1$. This corresponds to $z_L = 0.8$ and $z_R = 0.7$ and we assume that $\mu_L = \mu_R$. The computed density, temperature, and fugacity profiles are output at time $t = 0.25$ (dimensionless time) and the CFL number used is 1. We compare the results of the first order KFVS and high-order KFVS–WENO3 schemes with 200 cells.

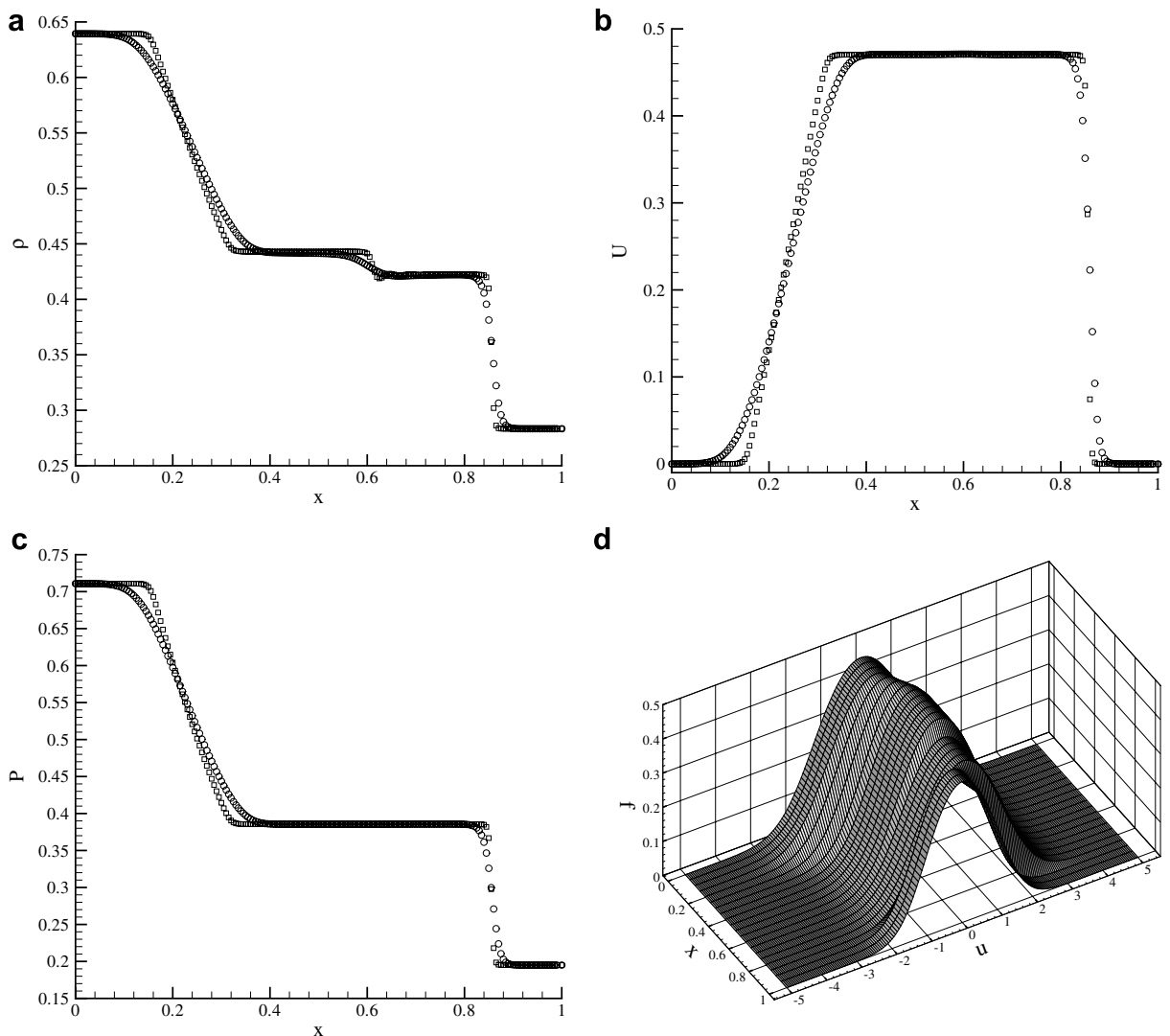


Fig. 2. Quantum shock tube solution, Fermi gas: 1st order (○) and WENO3 (□).

The expansion fan, contact line, and shock can be easily identified. As can be seen, the effect of high-order method is clearly depicted. A plot of Bose–Einstein distribution function at several stations at time $t = 0.25$ is also shown in Fig. 1d. Here, 21 lines are plotted for $0 \leq x \leq 1$ with equal spacing $\Delta x = 0.05$ and the range of u is $-5 \leq u \leq 5$. The distribution function profiles in the near classical limit at most stations are close to a Gaussian distribution as expected. The accuracy of the present KFVS–WENO3 is about fifth order in smooth region and third order at critical points similar to the conclusion presented by Henrick et al. The CPU times for the first order KFVS and KFVS–WENO3 are 9.234 and 94.109 s, respectively, on a 3.2 GHz personal computer on a 200 uniform grid system.

Example 2 (1D shock tube problem: fermion gas). The set up of the problem is the same as Example 1. The initial condition is specified as $\mathbf{W}_L = (\rho_L, \rho_L U_L, \rho_L \epsilon_L) = (0.639, 0.0, 1.066)$ for $0 < x \leq 0.5$ and $\mathbf{W}_R = (\rho_R, \rho_R U_R, \rho_R \epsilon_R) = (0.283, 0.0, 0.293)$ for $0.5 < x < 1$. This corresponds to $z_L = 0.8$ and $z_R = 0.7$ and we assume that $\mu_L = \mu_R$. The computed density, temperature, and fugacity profiles are output at time $t = 0.25$ (dimensionless time) and the CFL number used is 1. We compare the results that using first order KFVS and KFVS–WENO3 schemes with 200 cells. As can be seen, the various flow structures can be identified and the effect of high-order method is clearly depicted. The expected order of accuracy is similar to the above discussion given at Example 1. A plot of Fermi–Dirac distribution function at several stations at time $t = 0.25$ is also shown in Fig. 2d. Here, 21 lines are plotted for $0 \leq x \leq 1$ with equal spacing $\Delta x = 0.05$ and the range of u is $-5 \leq u \leq 5$.

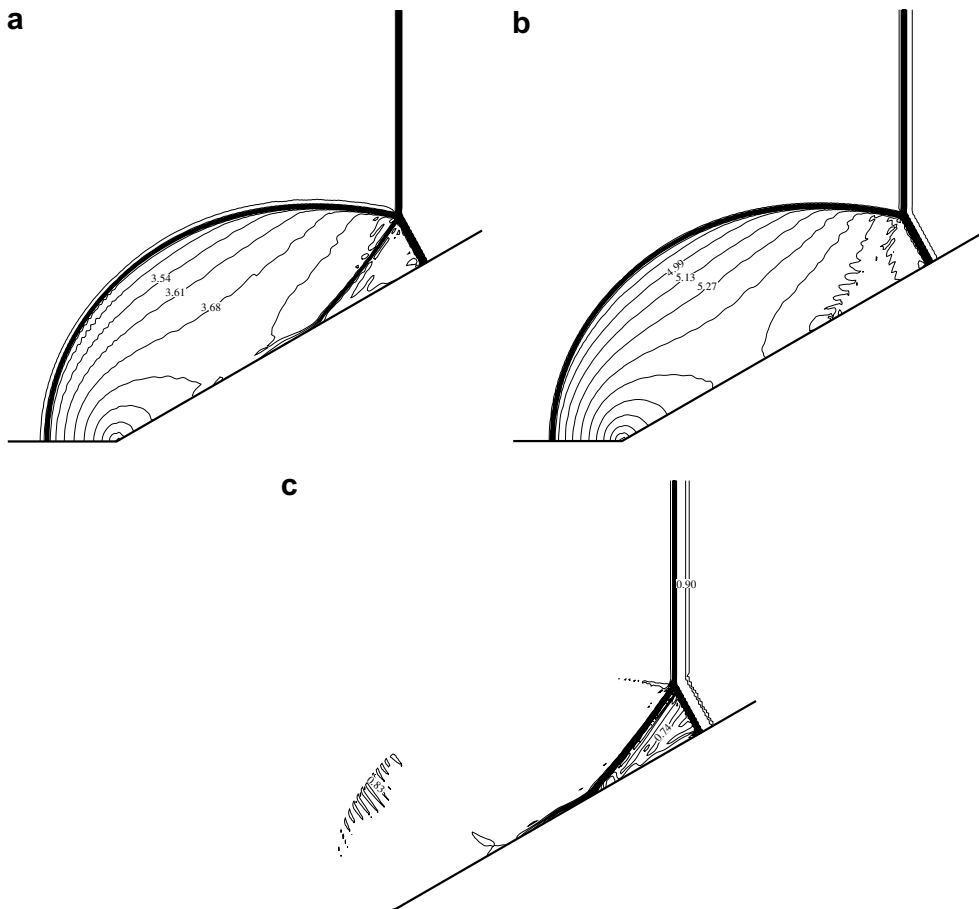


Fig. 3. Quantum shock reflection by a wedge, Bose gas: (a) density, (b) pressure, and (c) fugacity.

Example 3 (*Shock wave diffraction by a 2D wedge: boson gas*). We consider a plane moving shock wave located initially at a certain distance ahead of the inclined wedge with Mach number equal to $M_s = 2$ and the fugacity downstream is 0.9. The flow quantities of state 1 and 2 are $(\rho_1, U_1, \epsilon_1, T_1) = (1.266, 0.0, 1.140, 0.850)$ and $(\rho_2, U_2, \epsilon_2, T_2) = (2.894, 1.125, 7.244, 1.655)$, respectively. The computational domain is divided into two regions. Region 1 is ahead of the wedge with $0.0 \leq x \leq 1.0$ and $0.0 \leq y \leq 2.0$ and region 2 is above the wedge with $1.0 \leq x \leq 3.0$ and $y = (x - 1)\tan\theta(x - 1)\tan\theta + 2$. The mesh used in region 1 is $(x, y) = (i\Delta x, j\Delta y)$ and $(x, y) = (i\Delta x, (i\Delta x - 1)\tan\theta + j\Delta y)$ in region 2. The mesh size used is $\Delta x = \Delta y = 0.01$. Here, the case of wedge angle $\theta = 30^\circ$ is computed. We use WENO3–KFVS scheme with CFL = 0.1. In Fig. 3, the density, pressure and fugacity contour are shown for the instant of time $t = 0.7$ and 41 contour levels are used. The complex Mach reflection pattern is observed in this case and the reflected shock, the triple shock and Mach stem can be clearly identified.

Example 4 (*Shock wave diffraction by a 2D wedge: fermion gas*). The initial set up of the problem is the same as Example 3 with moving shock Mach number $M_s = 2$ and the downstream fugacity $z_2 = 0.9$. The flow quantities of state 1 and 2 are $(\rho_1, U_1, \epsilon_1, T_1) = (0.275, 0.0, 0.247, 0.534)$ and $(\rho_2, U_2, \epsilon_2, T_2) = (0.628, 1.125, 1.572, 1.144)$, respectively. The same computational domain and mesh system as Example 3 are employed. We use WENO3–KFVS scheme with CFL = 0.1. In Fig. 4, the density, pressure and fugacity contour are shown at time $t = 0.7$ and 41 contour levels are plotted. The flow patterns are similar to the previous case, namely, the complex Mach reflection type. All the flow features can be well presented by the present high-order KFVS method.

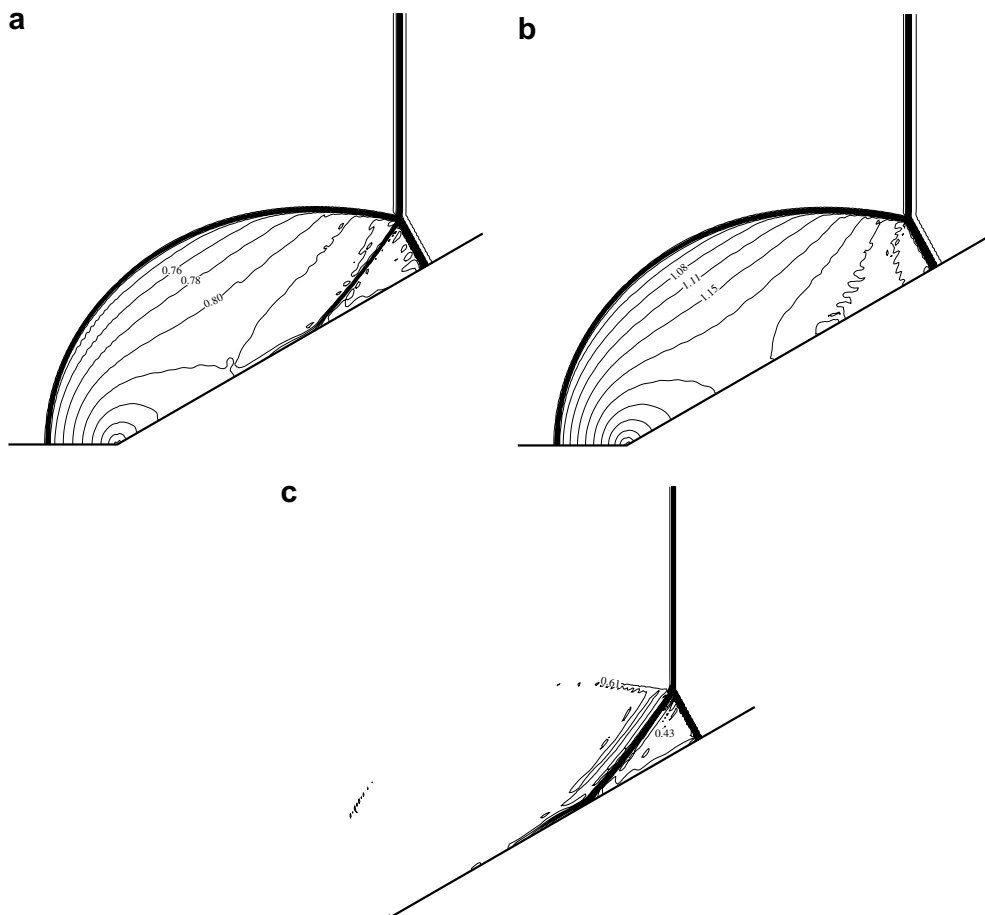


Fig. 4. Quantum shock wave reflection by a wedge, Fermi gas: (a) density, (b) pressure, and (c) fugacity.

Example 5 (*Shock wave diffraction by a 2D cylinder: boson gas*). In this problem, we consider a plane shock wave located initially at a certain distance (here $x = -0.7$) ahead of the circular cylinder that propagates with shock Mach number $M_s = 2.0$ toward the cylinder and experiences transient shock diffraction. A simple cylindrical grid system of 181×181 was used for half cylinder, consisting of 181 rays around the cylinder and 181 circles between the cylinder surface and outer boundary which is slightly stretched with $\Delta r_{\min} = .03$. The diameter of the cylinder is 1.0 and the distance between the origin of the cylinder and the outer boundary is 7.0. First, we report the results for the case of Bose–Einstein gas. The initial conditions are set as $M_s = 2.0$ and fugacity $z_1 = 0.9$. The flow quantities of state 1 and 2 are $(\rho_1, U_1, \epsilon_1, T_1) = (1.266, 0.0, 1.140, 0.850)$ and $(\rho_2, U_2, \epsilon_2, T_2) = (2.894, 1.125, 7.244, 1.655)$, respectively. The fugacity in state 2 is $z_2 = 0.833$. In Fig. 5, the density contours obtained by the KFVS–WENO3 scheme at a series of times are shown. In Fig. 5a, the incident shock is about to hit the cylinder surface and the density contour is constant on either side of the moving

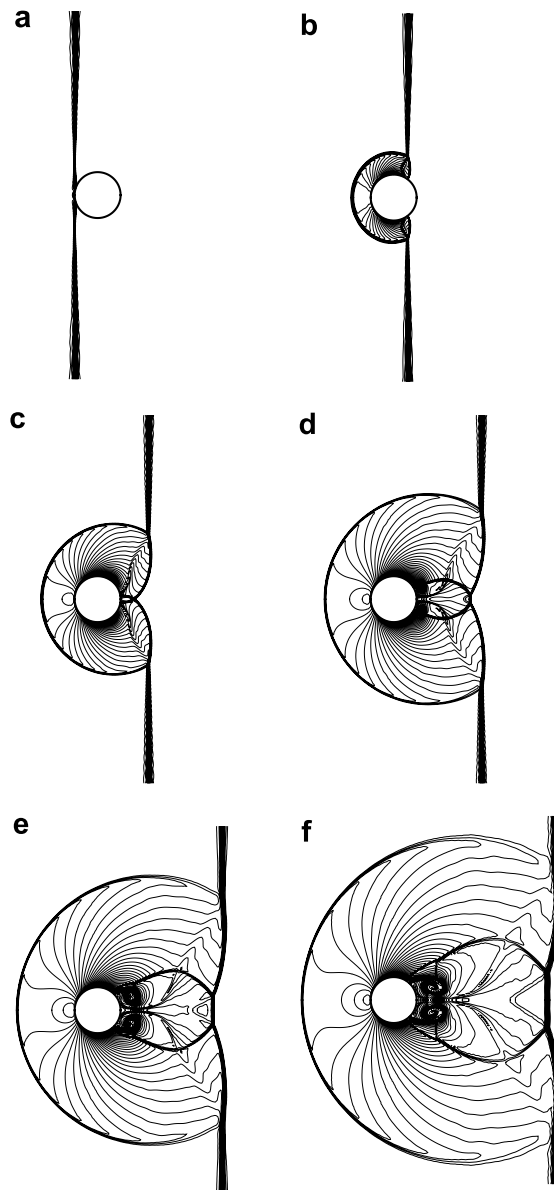


Fig. 5. Density contours of a shock diffraction by a circular cylinder: Bose gas.

shock. Fig. 5b–f shows the subsequent development of the diffraction process that covers regular reflection, transition to Mach reflection, the Mach shocks collision at the wake, and the complex shock on shock interaction. The primary incident shock, reflected bow shock, Mach shock, contact discontinuity, and vortex can be easily identified. It is observed that the complicated flow interaction resulting in Mach shocks, second contact discontinuities, and triple point can all be accurately represented.

Example 6 (*Shock wave diffraction by a 2D cylinder: fermion gas*). The initial set up of the problem and the grid system used are the same as Example 5. For the Fermi–Dirac gas, the initial conditions are set as $M_s = 2.0$ and fugacity $z_1 = 0.9$. The flow quantities of state 1 and 2 are $(\rho_1, U_1, \epsilon_1, T_1) = (0.275, 0.0, 0.247, 0.534)$ and $(\rho_2, U_2, \epsilon_2, T_2) = (0.628, 1.125, 1.572, 1.144)$, respectively. The fugacity in state 2 is $z_2 = 0.615$. In Fig. 6, the

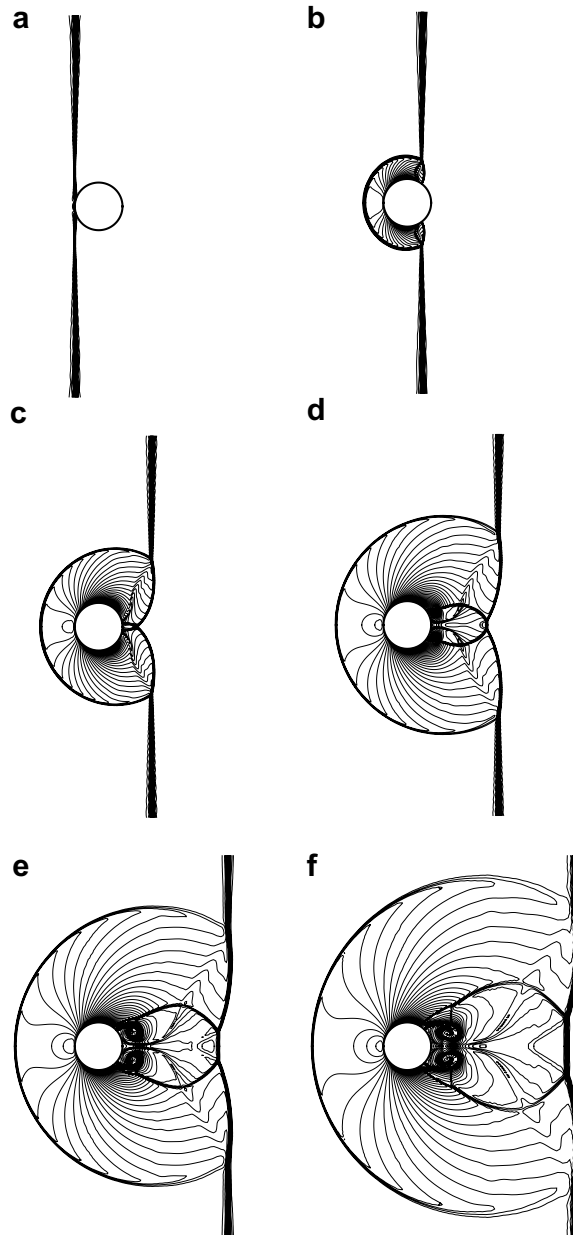


Fig. 6. Density contours of a shock diffraction by a circular cylinder: Fermi gas.

density contours obtained by the KFVS–WENO3 scheme at a series of times are shown. In Fig. 6a, the incident shock is about to hit the cylinder surface and the density contours is constant on either side of the moving shock. Fig. 6b–f shows the subsequent development of the diffraction process that covers regular reflection, transition to Mach reflection, the Mach shocks collision at the wake, and the complex shock on shock interaction. The primary incident shock, reflected bow shock, Mach shock, contact discontinuity, and vortex in the entire diffraction process can be easily identified. It is observed that the complicated flow features can be accurately captured by the present high-order quantum KFVS scheme.

6. Concluding remarks

In this work, the basic first order kinetic flux vector splitting method for ideal quantum gas dynamics has been derived based on an initial value problem of collisionless quantum Boltzmann equation. The present derivation is systematically done by starting with the general three-dimensional (in velocity or momentum space) equilibrium distribution function instead of using the reduced distribution function for lower dimensions. Both Bose–Einstein and Fermi–Dirac gases are considered. The formulations of the split fluxes are given for one- to three-dimensional problems. The basic first order KFVS scheme is entropy-satisfying and positive and thus is desirable for shock capturing. General curvilinear coordinates have been introduced to treat general geometries. Implementation of weighted essentially non-oscillatory method into the basic first order flux vector splitting to yield a class of high resolution schemes can be naturally done without using characteristic projection as in other approximate Riemann solvers. The resulting high-order KFVS schemes have been tested using 1D shock tube problem, unsteady shock wave diffraction by a 2D wedge, and unsteady shock wave diffraction by a circular cylinder. Accurate resolutions of the flow features in all cases have been obtained. The present method can provide a viable and robust tool for computing various ideal quantum gas dynamical flow problems.

Acknowledgments

This work is done under the auspices of National Science Council, Taiwan through Grants NSC 95-2221E002-055 and NSC 95-2212E002-089.

Appendix A

In this appendix, the formulations for the split fluxes in three-dimensional flow problems under curvilinear coordinates are given. Define the unit normal and the contravariant velocities as:

$$(\hat{\chi}_x, \hat{\chi}_y, \hat{\chi}_z) = \frac{(\chi_x, \chi_y, \chi_z)}{\sqrt{\chi_x^2 + \chi_y^2 + \chi_z^2}}, \quad \chi = \zeta, \eta, \xi, \tag{59}$$

$$\hat{U} = \hat{\xi}_x U + \hat{\xi}_y V + \hat{\xi}_z W, \quad \hat{V} = \hat{\eta}_x U + \hat{\eta}_y V + \hat{\eta}_z W, \quad \hat{W} = \hat{\zeta}_x U + \hat{\zeta}_y V + \hat{\zeta}_z W. \tag{60}$$

Then the split fluxes in the generalized coordinates (ξ, η, ζ) are given, respectively, by

$$\hat{F}^\pm = \begin{pmatrix} \hat{F}_\rho^\pm \\ \hat{F}_{\rho U}^\pm \\ \hat{F}_{\rho V}^\pm \\ \hat{F}_{\rho W}^\pm \\ \hat{F}_{\rho e}^\pm \end{pmatrix} = \begin{pmatrix} \rho \hat{U} a^\pm(\hat{U}) \pm \rho b(\hat{U}) \\ \hat{\xi}_x P c^\pm(\hat{U}) + U(\rho \hat{U} a^\pm(\hat{U}) \pm \rho b(\hat{U})) \\ \hat{\xi}_y P c^\pm(\hat{U}) + V(\rho \hat{U} a^\pm(\hat{U}) \pm \rho b(\hat{U})) \\ \hat{\xi}_z P c^\pm(\hat{U}) + W(\rho \hat{U} a^\pm(\hat{U}) \pm \rho b(\hat{U})) \\ \frac{5}{2} P \hat{U} c^\pm(\hat{U}) + 2 P d(\hat{U}) + \frac{1}{2}(U^2 + V^2 + W^2)(\rho \hat{U} a^\pm(\hat{U}) \pm \rho b(\hat{U})) \end{pmatrix}, \tag{61}$$

$$\hat{G}^\pm = \begin{pmatrix} \hat{G}_\rho^\pm \\ \hat{G}_{\rho U}^\pm \\ \hat{G}_{\rho V}^\pm \\ \hat{G}_{\rho W}^\pm \\ \hat{G}_{\rho \epsilon}^\pm \end{pmatrix} = \begin{pmatrix} \rho \hat{V} a^\pm(\hat{V}) \pm \rho b(\hat{V}) \\ \hat{\eta}_x P c^\pm(\hat{V}) + U(\rho \hat{V} a^\pm(\hat{V}) \pm \rho b(\hat{V})) \\ \hat{\eta}_y P c^\pm(\hat{V}) + V(\rho \hat{V} a^\pm(\hat{V}) \pm \rho b(\hat{V})) \\ \hat{\eta}_z P c^\pm(\hat{V}) + W(\rho \hat{V} a^\pm(\hat{V}) \pm \rho b(\hat{V})) \\ \frac{5}{2} P \hat{V} c^\pm(\hat{V}) + 2Pd(\hat{V}) + \frac{1}{2}(U^2 + V^2 + W^2)(\rho \hat{V} a^\pm(\hat{V}) \pm \rho b(\hat{V})) \end{pmatrix}, \quad (62)$$

$$\hat{H}^\pm = \begin{pmatrix} \hat{H}_\rho^\pm \\ \hat{H}_{\rho U}^\pm \\ \hat{H}_{\rho V}^\pm \\ \hat{H}_{\rho W}^\pm \\ \hat{H}_{\rho \epsilon}^\pm \end{pmatrix} = \begin{pmatrix} \rho \hat{W} a^\pm(\hat{W}) \pm \rho b(\hat{W}) \\ \hat{\zeta}_x P c^\pm(\hat{W}) + U(\rho \hat{W} a^\pm(\hat{W}) \pm \rho b(\hat{W})) \\ \hat{\zeta}_y P c^\pm(\hat{W}) + V(\rho \hat{W} a^\pm(\hat{W}) \pm \rho b(\hat{W})) \\ \hat{\zeta}_z P c^\pm(\hat{W}) + W(\rho \hat{W} a^\pm(\hat{W}) \pm \rho b(\hat{W})) \\ \frac{5}{2} P \hat{W} c^\pm(\hat{W}) + 2Pd(\hat{W}) + \frac{1}{2}(U^2 + V^2 + W^2)(\rho \hat{W} a^\pm(\hat{W}) \pm \rho b(\hat{W})) \end{pmatrix}, \quad (63)$$

where expressions of functions a^\pm , b , c^\pm , and d are given in Eqs. (21)–(24).

References

- [1] P.L. Bhatnagar, E.P. Gross, M. Krook, A model for collision process in gases I: small amplitude processes in charged and neutral one-component systems, *Phys. Rev.* 94 (1954) 511–525.
- [2] S. Chapman, T.G. Cowling, *The Mathematical Theory of Non-Uniform Gases*, Cambridge University Press, Cambridge, 1970.
- [3] G. Chen, *Nanoscale Energy Transport and Conversion*, Oxford University Press, Oxford, 2005.
- [4] S.Y. Chou, D. Baganoff, Kinetic flux-vector splitting for the Navier–Stokes equations, *J. Comput. Phys.* 130 (1997) 217–230.
- [5] S.M. Deshpande, A second order accurate, kinetic-theory based, method for inviscid compressible flows, NASA Langley Technical Paper No. 2613, 1986.
- [6] A.L. Garcia, W. Wagner, Direct simulation Monte Carlo method for the Uehling–Uhlenbeck–Boltzmann equation, *Phys. Rev. E* 68 (2003) 056703.
- [7] A.K. Henrick, T.D. Aslam, J.M.u. Powers, Mapped weighted essentially non-oscillatory schemes: achieving optimal order near critical points, *J. Comput. Phys.* 207 (2005) 542–567.
- [8] C. Hirsch, *Numerical Computation of Internal and External Flows*, Wiley, New York, 1988.
- [9] K. Huang, *Statistical Mechanics*, Wiley, New York, 1987.
- [10] G.-S. Jiang, C.-W. Shu, Efficient implementation of weighted ENO schemes, *J. Comput. Phys.* 126 (1996) 202–228.
- [11] L.P. Kadanoff, G. Baym, *Quantum Statistical Mechanics*, Benjamin, New York, 1962 (Chapter 6).
- [12] X.-D. Liu, S. Osher, T. Chan, Weighted essentially non-oscillatory schemes, *J. Comput. Phys.* 115 (1994) 200–212.
- [13] A. Minguzzi, S. Succi, F. Toschi, M.P. Tosi, P. Vignolo, Numerical methods for atomic quantum gases with applications to Bose–Einstein condensates and to ultracold fermions, *Phys. Rep.* 395 (2004) 223.
- [14] T. Ohwada, On the construction of kinetic schemes, *J. Comput. Phys.* 177 (2002) 156–175.
- [15] R.K. Pathria, *Statistical Mechanics*, second ed., Butterworths–Heinemann, London, 1996.
- [16] C.J. Pethick, H. Smith, *Bose–Einstein Condensation in Dilute Gases*, Cambridge University Press, Cambridge, 2002.
- [17] G.N. Patterson, *Introduction to the Kinetic Theory of Gas Flows*, University of Toronto Press, Toronto, 1971.
- [18] R.H. Sanders, K.H. Predergast, The possible relation of the 3-kiloparsec arm to explosions in the galactic nucleus, *Astrophys. J.* 188 (1974) 489.
- [19] E.F. Toro, *Riemann Solvers and Numerical Methods for Fluid Dynamics*, Springer, Berlin, 1999.
- [20] E.A. Uehling, G.E. Uhlenbeck, Transport phenomena in Bose–Einstein and Fermi–Dirac gases. I, *Phys. Rev.* 43 (1933) 552.
- [21] K. Xu, K.H. Predergast, Numerical Navier–Stokes solutions from gas kinetic theory, *J. Comput. Phys.* 114 (1994) 9–17.
- [22] K. Xu, Gas-kinetic schemes for unsteady compressible flow simulations, in: *Proceedings of the 29th Computational Fluid Dynamics Lecture Series*, von Karman Institute for Fluid Dynamics, Rhode-Saint-Geneses, Belgium, 1998.
- [23] K. Xu, A gas-kinetic BGK scheme for the Navier–Stokes equations and its connection with artificial dissipation and Godunov method, *J. Comput. Phys.* 171 (2001) 289–335.
- [24] Z. Xu, C.-W. Shu, Anti-diffusive flux corrections for high order finite difference WENO schemes, *J. Comput. Phys.* 205 (2005) 458–485.
- [25] J.Y. Yang, Y.H. Shi, A kinetic beam scheme for ideal quantum gas dynamics, *Proc. Roy. Soc. Lond. A* 462 (2006) 1553–1572.
- [26] J.Y. Yang, T.Y. Hsieh, Y.H. Shi, Kinetic flux splitting schemes for ideal quantum gas dynamics, *SIAM J. Sci. Comput.* 29 (2007) 221–244.